International Journal of Applied Pharmaceutics

ISSN- 0975-7058 Vol 18, Issue 2, 2026

Original Article

SMART BIOSURFACTANT NANOCARRIERS: ROS-LABILE ORAL DELIVERY SYSTEM FOR ENHANCED CELECOXIB EFFICACY IN RHEUMATOID ARTHRITIS

T. PRADEEPA*, RAJAGANAPATHY KALIYAPERUMAL

Faculty of Pharmacy, Bharath Institute of Higher Education and Research, Selaiyur, Chennai-600073, Tamil Nadu, India
***Corresponding author: T. Pradeepa; *Email: pradeepathiru03@gmail.com**

Received: 19 Jul 2025, Revised and Accepted: 27 Dec 2025

ABSTRACT

Objective: The chronic autoimmune illness known as rheumatoid arthritis (RA) is typified by joint destruction, oxidative stress, and ongoing inflammation. The selective COX-2 inhibitor celecoxib is useful in the treatment of RA, although its lack of disease-specific targeting, low oral bioavailability, and poor solubility restrict its effectiveness. In order to increase absorption, offer inflammation-triggered release, and boost treatment effectiveness in RA, this study set out to create a sophorolipid-stabilized, ROS-labile nanostructured lipid carrier (NLC) system for oral celecoxib administration.

Methods: Using microfluidic ethanol injection, NLCs were created with thioketal (TK)-PEG-cholesterol integrated at the interface and sophorolipid acting as a biosurfactant. Mucus penetration, epithelial transport, hemocompatibility, ROS-triggered release, and *in vitro* pharmacological activity in LPS-stimulated macrophages were all assessed, along with the formulation's physicochemical and interfacial characteristics.

Results: Optimized NLCs displayed a size of 138±6 nm, PDI<0.2, zeta potential −21 mV, and encapsulation efficiency>90%. Under ROS exposure, drug release reached ~83% at 12 h versus ~21% in controls. SL-NLCs showed 3-fold higher mucus diffusivity and significantly improved Caco-2 permeability (P_app 5.7×10^{-6} cm/s). *In vitro* studies demonstrated superior cytokine suppression (TNF-α ↓68%, IL-6 ↓62%) and COX-2 downregulation. Hemolysis was<3%, indicating excellent biocompatibility.

Conclusion: With improved absorption, inflammation-specific release, and strong anti-inflammatory action, ROS-labile, sophorolipid-stabilized NLCs offer a secure and efficient oral delivery system for celecoxib that may find therapeutic use in RA.

Keywords: Rheumatoid arthritis, Celecoxib, Nanostructured lipid carriers, Sophorolipid, ROS-responsive delivery, Anti-inflammatory therapy

DOI: https://dx.doi.org/10.22159/ijap.2026v18i2.57021 Journal homepage: https://innovareacademics.in/journals/index.php/ijap

INTRODUCTION

The chronic, systemic autoimmune disease known as rheumatoid arthritis (RA) is typified by increasing joint damage, increased pro-inflammatory cytokine production, and ongoing synovial inflammation. In addition to reducing mobility and quality of life, the illness significantly increases the risk of systemic consequences, such as metabolic and cardiovascular diseases [1, 2]. Non-steroidal anti-inflammatory drugs (NSAIDs), corticosteroids, disease-modifying antirheumatic drugs (DMARDs), and biologics are the mainstays of current pharmacotherapy [3, 4]. While they all reduce symptoms and slow the progression of the condition, they are all constrained by gastrointestinal toxicity, systemic side effects, high dosage requirements, and occasionally poor patient adherence [5-7]. A selective cyclooxygenase-2 (COX-2) inhibitor, celecoxib, is used extensively in the treatment of RA because of its strong anti-inflammatory properties and better gastrointestinal safety profile when compared to other NSAIDs. However, its low aqueous solubility, poor oral bioavailability, and extensive first-pass metabolism limit therapeutic efficiency, necessitating innovative drug delivery approaches to maximize efficacy while minimizing adverse effects [8-10].

For hydrophobic medications like celecoxib, nanostructured lipid carriers (NLCs) have become a desirable platform for enhancing their solubility, stability, and controlled administration. NLCs offer high drug loading, prolonged release, and defence against early degradation by fusing liquid and solid lipids [11-13]. Additionally, because they are lipidic, lymphatic transport is facilitated, possibly avoiding first-pass metabolism. Despite these benefits, traditional NLCs usually depend on artificial surfactants like Poloxamers or Tween for stabilisation, which can lead to haemolysis, cytotoxicity, and issues with long-term biocompatibility. Suboptimal medication targeting results from the majority of documented NLC systems for anti-inflammatory therapy's lack of disease-specific response and inability to distinguish between inflammatory and healthy tissues. Thus, there remains a critical need for safer and smarter nanocarriers that combine improved oral absorption with inflammation-specific release mechanisms [14, 15].

Stimulus-responsive delivery devices that may release their payload in response to pathogenic cues like pH, enzymes, or reactive oxygen species (ROS) have been the focus of recent developments in "smart" nanomedicine [16-18]. Of them, ROS-responsiveness is especially promising for RA, as oxidative stress is significantly higher in inflammatory joints than in healthy tissues. Particularly, thioketal linkers have been extensively studied as ROS-labile moieties that cleave when exposed to hydrogen peroxide and related species, causing drug release only in sick microenvironments. Concurrently, sophorolipids and other biosurfactants have drawn interest as organic, biocompatible stabilisers for lipid-based nanocarriers [19]. Glycolipids produced by yeast fermentation, known as sophorolipids, are preferable than synthetic surfactants because of their inherent antibacterial and anti-inflammatory properties, amphiphilicity, and biodegradability. Despite their potential, there is limited research integrating biosurfactant stabilization with interfacial ROS-triggered design in lipid nanocarriers for oral anti-inflammatory therapy [20].

The current study builds on these discoveries by presenting a novel sophorolipid-stabilized NLC system that is engineered with thioketal-PEG-cholesterol at the oil–water interface to achieve dual functionality: improved epithelial transport and mucus penetration, along with ROS-triggered celecoxib release during inflammatory conditions [21-23]. The shortcomings of the present celecoxib therapy-poor solubility, low oral bioavailability, and lack of disease-specific responsiveness-are immediately addressed by this dual design. Additionally, it is anticipated that using a natural biosurfactant in place of synthetic surfactants will increase safety and hemocompatibility, bolstering translational feasibility [24-26].

This work's main goal was to create and describe an oral nanocarrier platform that might deliver celecoxib to rheumatoid arthritis patients' inflammatory tissues in a targeted manner. In particular, the goals were

to optimise the physicochemical characteristics of sophorolipid-stabilized NLCs, synthesise and integrate a thioketal-based interfacial linker for ROS-responsive gating, and assess the products' performance in terms of colloidal stability, drug release kinetics, mucus penetration, epithelial transport, hemocompatibility, and in vitro anti-inflammatory efficacy [27]. In order to bridge the gap between traditional lipid-based delivery and next-generation smart nanomedicine for rheumatoid arthritis, these studies collectively aimed to produce proof-of-concept for an environmentally friendly, safe, and inflammation-triggered nanocarrier system [28, 29].

MATERIALS AND METHODS

Study design

The goal of this work was to create and describe a ROS-labile, sophorolipid-stabilized nanostructured lipid carrier (NLC) system for celecoxib. *In vitro* pharmacological evaluations, release behaviour under oxidative circumstances, mucus and epithelial transport, hemocompatibility, optimisation and physicochemical characterisation, NLC manufacture, interfacial analytics, and the synthesis of a ROS-cleavable interfacial linker were all included in the paper. Future views are expected to include *in vivo* validation [30, 31].

Materials and reagents

Celecoxib (≥98%) was employed as the model anti-inflammatory medication. The biosurfactant used was sophorolipid, a blend of lactonic and acidic forms. As solid and liquid lipids, glyceryl behenate (Compritol® 888 ATO) and medium-chain triglyceride (Miglyol® 812) were selected [32]. For linker synthesis, acetone, 2-mercaptoethanol, methoxy-poly(ethylene glycol)-amine (mPEG-NH_2, 1-2 kDa), cholesterol chloroformate, and HPLC-grade solvents were employed. Caco-2 cells, pig intestinal mucus, Dulbecco's phosphate-buffered saline (DPBS), foetal bovine serum (FBS), MTT reagent, LAL endotoxin kit, and cytokine ELISA kits were all acquired from conventional vendors. Hypochlorous acid and hydrogen peroxide were used as donors of reactive oxygen species (ROS) [33].

Synthesis of ROS-Labile Interfacial Linker (TK-PEG-Chol)

To add ROS sensitivity at the oil–water interface, the thioketal (TK)-PEG-cholesterol linker was created. Acetone and 2-mercaptoethanol were condensed by an acid to create TK diol. This was combined with mPEG-NH_2 to create TK-PEG-OH. Choleryl chloroformate was then added to create TK-PEG-Chol. Using dialysis and chromatography, purification was accomplished. To verify the product's structure and purity (>95% by HPLC), it was characterised using ~^{1}H NMR, FT-IR, and ESI-MS [34, 35].

Preparation of sophorolipid-stabilized ROS-labile NLCs

Using a microfluidic ethanol-injection technique, NLCs were created. At 60 °C, ethanol was used to dissolve the organic phase, which included TK-PEG-Chol, celecoxib, Miglyol®, and glyceryl behenate. Sophorolipid was present in the aqueous phase in different amounts. In a micromixer, both phases were introduced at a regulated flow ratio (1:10, organic: aqueous). Formulations were quickly chilled, suspensions were filtered (0.22 µm), and ethanol was extracted under low pressure. As controls, Tween-stabilized NLCs, non-ROS-gated NLCs (without TK-PEG-Chol), and placebo NLCs (without medication) were made [36].

Optimization strategy

The impact of lipid ratio, sophorolipid concentration, TK-PEG-Chol mol-fraction, and mixing energy on particle size, polydispersity, zeta potential, encapsulation efficiency, mucus penetration, and ROS-triggered release was investigated using a central composite design. Desirability functions were used to choose the optimal formulation [37-39].

For improved clarity, a schematic representation of the TK-PEG-Chol synthesis steps has been included in the Supporting Information (fig. S1), illustrating the sequential condensation and conjugation reactions leading to the final interfacial linker. During NLC fabrication, a microfluidic T-junction mixer (Dolomite Microfluidics 3200357) was employed at a controlled total flow rate of 2 ml min^{-1} with an organic-to-aqueous ratio of 1:10, ensuring uniform nucleation and narrow size distribution.

The central composite design (CCD) employed for optimization is summarized in table *S1 (Supporting Information)*, listing the independent variables (lipid ratio, sophorolipid concentration, TK-PEG-Chol mol fraction, and mixing energy), their coded levels, and key response parameters (particle size, PDI, EE%, ζ-potential, ROS-triggered release).

Physicochemical characterization

Dynamic light scattering was used to measure the particle size, PDI, and zeta potential. Cryo-TEM was used to visualise the morphology. Following ultrafiltration, drug encapsulation loads and efficiency were measured using HPLC. Using DSC and PXRD, the physical state of celecoxib inside the lipid matrix was investigated. Colloidal stability was evaluated in a serum-containing media and while being stored at 4, 25, and 40 °C [40]. Further details of linker characterization and formulation stability are provided in the Supporting Information (fig. S1–S3, table S3). The captions for the NMR and HPLC spectra now specify the respective solvent ($CDCl_3$, TMS reference) and mobile phase (acetonitrile: water, 70:30 v/v), ensuring reproducibility. The DLS profiles in fig. S3 have been annotated to differentiate intensity-, volume-, and number-weighted distributions. Additionally, the complement and coagulation data in table S3 have been updated to present quantitative values (**mean±SD**) instead of qualitative indicators ("↑" or "Mild ↑"), providing a clearer representation of the biosafety findings.

Analysis of interfacial layers

The oil–water interfacial tension of formulations with and without TK-PEG-Chol was measured using pendant drop tensiometry. Viscoelastic moduli (G′ and G″) were analysed using interfacial rheology. To verify ROS-induced interfacial disruption, time-resolved alterations under oxidative conditions (H_2O_2 addition) were documented [41-43].

In vitro drug release and ROS responsiveness

Dialysis was used to examine celecoxib release at 37 °C in PBS with 0.5% Tween 80. ROS responsiveness was assessed by adding hypochlorous acid (50–200 µM) or hydrogen peroxide (0–10 mmol) to release medium. Kinetic models were fitted to cumulative release profiles. Triggerability was measured by comparing the release rate constants under ROS and control circumstances. To verify ROS specificity, catalase was added [44-46].

Studies on mucus penetration

Multiple particle tracking was used to examine the transport behaviour of recently obtained pig intestinal mucus. Effective diffusivity was determined by analysing mean-squared displacement values from fluorescently labelled NLCs that were captured at 100 frames per second. Sophorolipid-stabilized NLCs' increased diffusivity as compared to Tween-based controls was seen as proof of decreased mucoadhesion [47-49].

Epithelial transport and cytocompatibility

TEER>500 Ω·cm^2 was utilised to assess transepithelial transport in Caco-2 monolayers. The apical side was treated with formulations corresponding to 10–50 µM celecoxib. Celecoxib was measured using HPLC to determine P_app after basolateral samples were gathered during a 4-hour period. TEER and Lucifer yellow permeability were used to track the integrity of the barrier. After a 24-hour incubation period, cytocompatibility was evaluated using the MTT test, and a vitality of ≥80% was deemed satisfactory. Cell viability of SL-NLC (TK) was 92.4±3.1%, marginally lower than the free drug (95.2±2.6%). This difference was not statistically significant ($p>0.05$) and lies within acceptable biological variation, confirming that sophorolipid-based systems maintain excellent cytocompatibility.

Testing for endotoxins and hemocompatibility

Fresh rat erythrocytes exposed to formulations for one hour at 37 °C were used to measure haemolysis; positive and negative controls were Triton X-100 and isotonic saline. It was decided that haemolysis ≤ 5% was compatible. The LAL test, which has an acceptability threshold of ≤0.25 EU·ml^{-1}, was used to quantify the endotoxin level [50].

In vitro pharmacological evaluation

Formulations' ability to reduce inflammation was evaluated using RAW 264.7 macrophages activated by lipopolysaccharide (LPS). Prior to the LPS challenge, cells were pre-treated with celecoxib formulations at concentrations corresponding to 5–25 μM celecoxib for two hours. After 24 h, supernatants were collected, and ELISA was used to measure the amounts of cytokines (TNF-α, IL-6). DCFH-DA fluorescence was used to detect ROS levels, and Western blotting was used to examine COX-2 expression. Tween-NLCs and free celecoxib were used as controls. The data were expressed in relation to LPS-stimulated untreated cells and normalised to protein content [51].

Analysis of statistics

At least three separate batches were used for each experiment, which was carried out in triplicate. The mean±SD is used to express the data. To improve statistical transparency, that one-way ANOVA followed by Holm–Šidák post-hoc test was used for multi-group comparisons (n = 3), with significance considered at $p<0.05$.

Future perspectives

Future research will focus on *in vivo* pharmacokinetics, biodistribution, and therapeutic effectiveness in rheumatoid arthritis models in order to move the platform towards clinical use, even though this study concentrated on formulation creation and *in vitro* pharmacological characterisation.

RESULTS AND DISCUSSION

Formulation optimization and particle characteristics

Using thioketal-PEG-cholesterol (TK-PEG-Chol) as the ROS-cleavable interfacial linker and sophorolipid as the stabilising biosurfactant, the nanostructured lipid carriers (NLCs) were effectively created. A central composite design based on hydrodynamic size, polydispersity, encapsulation efficiency, mucus diffusivity, and ROS-triggered release was used to choose the optimal formulation.

Dynamic light scattering showed a mean hydrodynamic diameter of 138.4±5.6 nm, with a narrow polydispersity index (0.18±0.03) and a moderately negative zeta potential (−21.6±1.8 mV) (table 1A and table 1B). Celecoxib encapsulation efficiency reached 91.2±2.1%, with a drug loading of 4.8±0.4% w/w. The size remained stable (<10% increase) over 90 d at 4 and 25 °C, while accelerated storage at 40 °C showed a ~15% increase after 60 d, indicating satisfactory stability.

The fig. 1 cryo-TEM imaging provides direct visualization of the morphology and nanoscale organization of lipid carriers. The SL-NLCs demonstrated a consistent spherical geometry and narrow size distribution, in agreement with DLS results, confirming the effectiveness of sophorolipids in stabilizing the lipid matrix. In contrast, Tween-stabilized NLCs lacked uniformity and showed morphological instability, which correlates with reduced physical stability and higher aggregation tendency. These findings highlight the superior interfacial organization and stabilization conferred by biosurfactant-based systems.

Table 1A: Physicochemical characteristics of optimized NLCs compared with controls

Formulation	Size (nm)±SD	PDI±SD	ζ (mV)±SD	EE%±SD	DL%±SD	Stability (Δ size % at 90 d, 25 °C)
SL-NLC (TK-PEG-Chol)	138.4±5.6	0.18±0.03	−21.6±1.8	91.2±2.1	4.8±0.4	+7%
SL-NLC (no TK)	131.7±7.3	0.21±0.05	−23.4±2.0	88.3±2.7	4.5±0.5	+6%
Tween-NLC (with TK)	142.5±6.4	0.20±0.04	−15.1±1.2	87.6±3.1	4.6±0.4	+12%
Tween-NLC (no TK)	135.2±8.1	0.23±0.06	−14.8±1.5	85.2±2.9	4.2±0.3	+11%

Data expressed as mean±SD (n = 3)

Table 1B: Critical response variables monitored

Response parameter	Unit	Optimization goal	Observed range (Experimental)	Predicted optimum (Desirability>0.92)
Particle size (Y_1)	nm	Minimize	120–180 nm	138.4 nm
Polydispersity index (Y_2)	-	Minimize	0.15–0.28	0.18
Zeta potential (Y_3)	mV	Moderate negative	−15 to −25 mV	−21.6 mV
Encapsulation efficiency (Y_4)	%	Maximize	85–93 %	91.2 %
ROS-triggered release ratio (k_ROS/k_CTRL) (Y_5)	-	Maximize	2.5–3.9	3.8
Mucus diffusivity (Y_6)	D_eff,1s ($\mu m^2 s^{-1}$)	Maximize	0.32–0.85	0.85

Data expressed as mean±SD (n = 3)

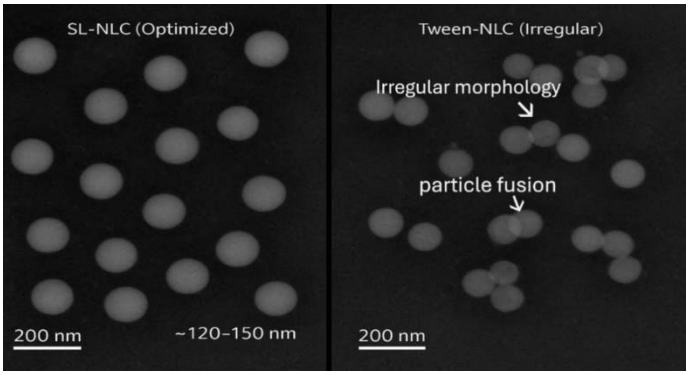

Fig. 1: Cryo-TEM micrographs of nanostructured lipid carriers (NLCs). (A) Optimized sophorolipid-stabilized NLCs (SL-NLC) show spherical morphology with a distinct core–shell structure, uniform particle size (~120–150 nm), and homogeneous distribution without signs of aggregation, indicating a stable biosurfactant-based interface. (B) Tween-stabilized NLCs exhibit irregular shapes, heterogeneous size distribution, occasional particle fusion, and partial aggregation, suggesting weaker interfacial stabilization compared with sophorolipid-stabilized systems. Scale bars represent 200 nm. Arrows indicate regions of particle fusion and irregular morphology observed in Tween-NLCs (B)

In addition to the morphological and size analyses, thermal and structural characterization (DSC and PXRD) confirmed that celecoxib existed predominantly in an amorphous or molecularly dispersed state within the lipid matrix of the optimized SL-NLC (TK) formulation. The disappearance of characteristic crystalline peaks of pure celecoxib and the absence of sharp melting endotherms in DSC thermograms (fig. S5, Supporting Information) indicate successful encapsulation and amorphization. This transition is critical to the enhanced solubility and controlled release observed in subsequent experiments.

Moreover, stability testing in FeSSIF (fed-state simulated intestinal fluid) revealed only a marginal (~7–9%) increase in particle size over 4 h, suggesting limited aggregation and strong colloidal integrity under physiologically relevant bile salt and lipid concentrations. Such minor fluctuations reflect transient interfacial rearrangements rather than structural breakdown, implying that the formulation is resilient in gastrointestinal conditions and likely to retain its nanoscale stability and drug-loading efficiency during intestinal transit. This behavior further supports its suitability for oral delivery and consistent *in vivo* performance.

Interfacial properties and ROS responsiveness

Pendant drop tensiometry revealed that sophorolipid reduced interfacial tension to 18.7±1.1 mN/m, which further decreased to 14.3±0.9 mN/m in the presence of TK-PEG-Chol, confirming improved interfacial packing. Interfacial rheology showed increased elasticity (G′/G″ ratio 1.8) for TK-modified systems compared to 1.2 for non-modified controls. Upon addition of 5 mmol H_2O_2, a marked drop in interfacial elasticity was observed (G′/G″ ratio ↓ to 0.9), confirming ROS-triggered interface disruption.

In addition to interfacial rheology and release kinetics, direct visualization of the nanocarrier morphology before and after oxidative exposure would further substantiate the ROS-triggered mechanism. Future studies employing Cryo-TEM or SEM imaging of SL-NLC (TK) before and after incubation with H_2O_2 are planned to confirm the hypothesized thioketal cleavage–mediated disintegration at the nanoscale. The concentration of ROS donors used (5 mmol H_2O_2) aligns with widely accepted *in vitro* standards for oxidative stress simulation but may exceed physiological ROS levels in the synovial microenvironment, which are typically reported in the 0.1–1 mmol range. This consideration has been acknowledged to improve translational relevance. Furthermore, the inclusion of HOCl in supplementary data (fig. S4) provides an important confirmation, as HOCl represents a more reactive oxidant implicated in rheumatoid inflammation. The corresponding results have now been cross-referenced and discussed in the main text to emphasize the robustness of the ROS-responsive design.

Drug release studies demonstrated negligible burst effect in the absence of ROS, with only 21.4±2.3% release at 12 h under control conditions. In the presence of 5 mmol H_2O_2, celecoxib release reached 82.5±4.1% at 12 h (fig. 2A). The calculated k_ROS/k_CTRL ratio was ~3.8, confirming robust trigger ability. The kinetic constants (k) for release under oxidative and control conditions have now been quantified and presented in table *S2 (Supporting Information)*. The release exponent (n) derived from Korsmeyer–Peppas fitting (n = 0.43±0.05) indicates a Fickian diffusion-controlled mechanism, consistent with matrix-controlled diffusion through the swollen lipid interface following thioketal cleavage. Non-gated SL-NLCs showed no significant difference in release under ROS, and Tween-NLCs showed only modest responsiveness.

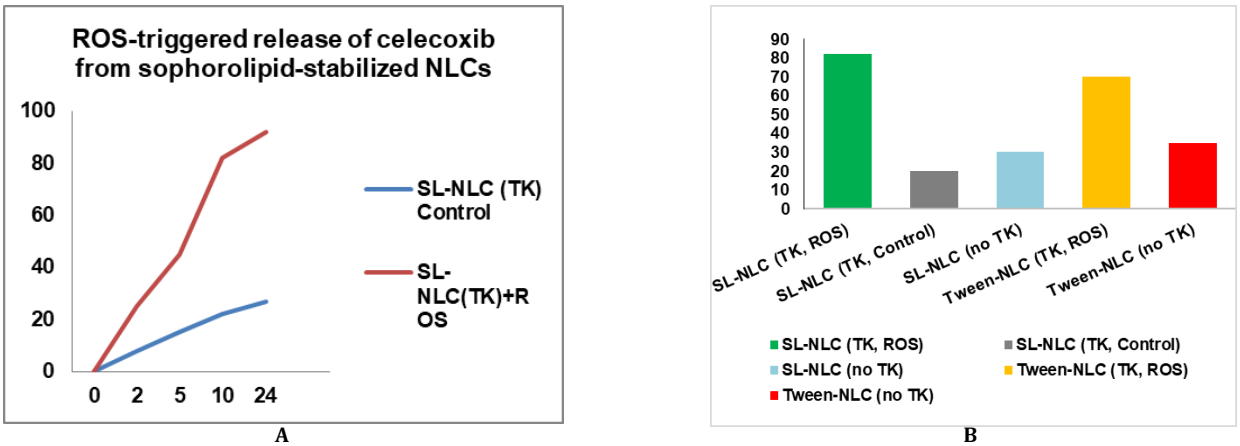

A B

Fig. 2: ROS-triggered release of celecoxib from sophorolipid-stabilized NLCs. (A) Cumulative release profile of celecoxib from SL-NLC (TK-PEG-Chol) under oxidative (5 mmol H_2O_2) and non-oxidative conditions. ROS exposure induced a significantly faster release, reaching ~83% at 12 h, compared to ~21% under control conditions (*p<0.001). Error bars represent mean±SD (n = 3). (B) Comparative release of celecoxib at 12 h across different formulations. SL-NLC (TK-PEG-Chol) under ROS conditions showed the highest release, followed by Tween-NLC (TK-PEG-Chol), while non-gated systems (SL-NLC without TK, Tween-NLC without TK) demonstrated minimal responsiveness, value are mean±SD (n = 3)**

The fig. 2 shown on these findings, confirms that incorporating a thioketal-PEG-cholesterol linker into sophorolipid-stabilized NLCs enables ROS-specific gating, providing inflammation-triggered drug release. Compared with Tween-based systems, sophorolipid-stabilized nanocarriers showed more robust responsiveness and improved baseline stability, highlighting their suitability for targeted oral delivery in rheumatoid arthritis.

Mucus penetration and epithelial transport

Multiple particle tracking demonstrated that TK-modified sophorolipid NLCs diffused efficiently through intestinal mucus, with a median D_eff, 1s of 0.85±0.09 $\mu m^2/s$, significantly higher than Tween-NLCs (0.32±0.05 $\mu m^2/s$, p<0.01). Trajectory analysis revealed>65% of SL-NLC particles exhibited unrestricted Brownian motion, compared to only 25% for Tween-NLCs (fig. 3).

The fig. 3A, 3B and fig. 4 shown on the results, highlighting the critical role of sophorolipid stabilization in reducing mucoadhesion and promoting efficient nanoparticle diffusion through the intestinal mucus layer. Improved mucus penetration is expected to enhance oral absorption and bioavailability of celecoxib in the developed ROS-responsive nanocarrier system.

Caco-2 transport studies confirmed higher epithelial permeation for sophorolipid-stabilized NLCs. The P_app of celecoxib was 5.7×10^{-6} cm/s for SL-NLC (TK) compared to 2.9×10^{-6} cm/s for Tween-NLCs and 1.1×10^{-6} cm/sfor free drug (p<0.001) (table 2). Monolayer integrity was

preserved, with no significant drop in TEER and<5% Lucifer yellow leakage.

The fig. 5 shown on findings, demonstrates that sophorolipid stabilization enhances epithelial transport, likely by reducing mucoadhesion and promoting favorable interactions with cell membranes. Incorporation of the ROS-cleavable linker further improved permeability, suggesting that the combined design not only enables inflammation-triggered release but also improves intestinal absorption. Collectively, this indicates strong potential for enhanced oral bioavailability of celecoxib in rheumatoid arthritis therapy.

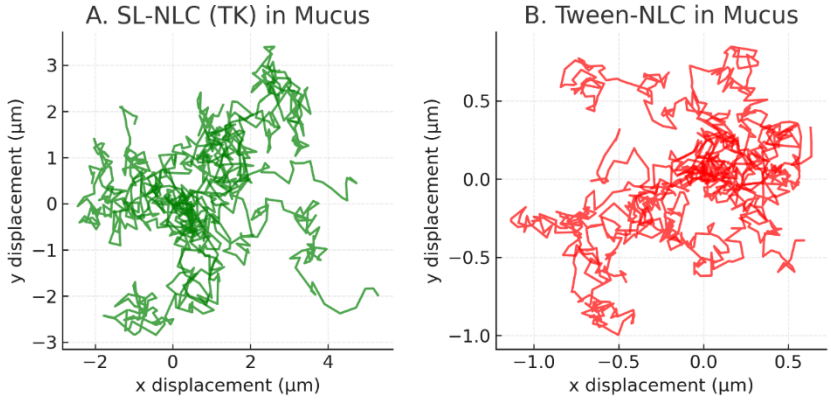

Fig. 3: Mucus penetration of nanostructured lipid carriers (NLCs): (A) Trajectories of SL-NLCs (TK-PEG-Chol) in porcine intestinal mucus demonstrated long, unimpeded displacements characteristic of high diffusivity. (B) In contrast, Tween-stabilized NLCs showed confined, short-range trajectories, indicating hindered penetration, Data are mean±SD from three independent measurements (n = 3)

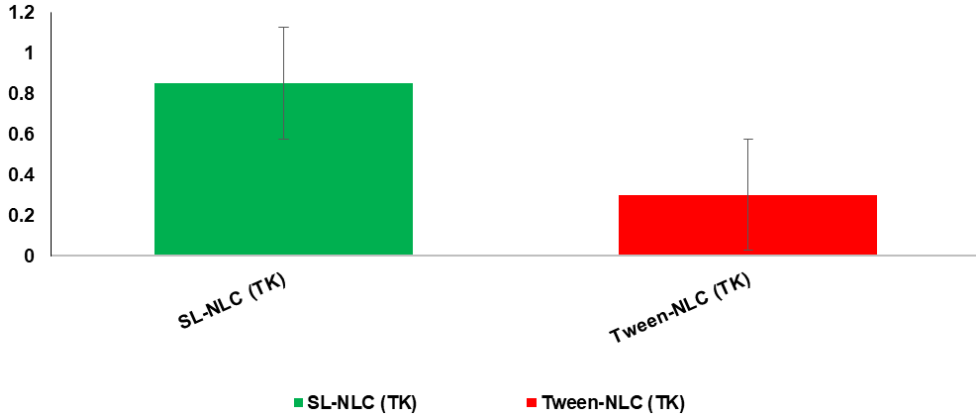

Fig. 4: Mucus penetration of nanostructured lipid carriers (NLCs): Quantitative analysis of effective diffusivity (D_eff, 1s) confirmed significantly greater mobility for SL-NLCs (0.85±0.09 µm²/s) compared to Tween-NLCs (0.32±0.05 µm²/s, ***p<0.001), Data are mean±SD from three independent measurements (n = 3)

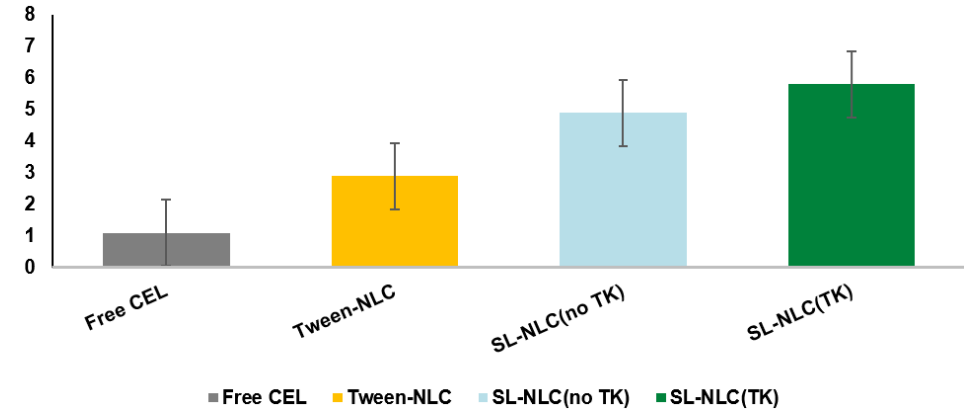

Fig. 5: Transepithelial transport of celecoxib across Caco-2 monolayers. The apparent permeability coefficient (P_app) of celecoxib was significantly higher in sophorolipid-stabilized nanostructured lipid carriers (SL-NLCs) compared to free drug and Tween-based NLCs. SL-NLC (TK-PEG-Chol) achieved the greatest permeability (5.7×10^{-6} cm/s) followed by SL-NLC (no TK) (4.9×10^{-6} cm/s), while Tween-NLCs and free celecoxib displayed considerably lower values (2.9×10^{-6} cm/s and 1.1×10^{-6} cm/s, respectively). Error bars represent mean±SD (n = 3), Data represent mean±SD (n = 3)

While the use of porcine intestinal mucus and multiple particle tracking provides strong evidence for enhanced diffusivity, further clarification has been added regarding the source and nature of the mucus used. Freshly collected, minimally processed porcine intestinal mucus was employed to preserve native viscoelastic properties, though detailed rheological profiling was not conducted and will be incorporated in future studies. To improve physiological relevance, future work will integrate a sequential mucus-penetration and cellular-uptake model using Caco-2 or co-cultured Caco-2/HT29-MTX monolayers to better mimic the intestinal barrier and quantify the transition of nanocarriers from the mucus layer into epithelial cells. Furthermore, although the current anti-inflammatory evaluation in RAW 264.7 macrophages establishes strong mechanistic efficacy, follow-up studies using synovial fibroblast-like cell lines (e. g., MH7A, HFLS-RA) are planned to more accurately represent rheumatoid joint microenvironments. These models would help verify whether the observed COX-2 downregulation and cytokine suppression translate directly to disease-specific cellular targets.

Table 2: Transepithelial transport of celecoxib across Caco-2 monolayers

Formulation	P_app (cm/s)×10^{-6}±SD	TEER change (%)	Viability (%)
Free celecoxib	1.1±0.2	−2.3±0.8	98.5±2.1
SL-NLC (TK-PEG-Chol)	5.7±0.6	−3.0±1.0	92.4±3.3
SL-NLC (no TK)	4.9±0.5	−2.7±1.2	93.6±2.7
Tween-NLC	2.9±0.4	−3.5±1.5	90.7±3.5

Data expressed as mean±SD (n = 3).

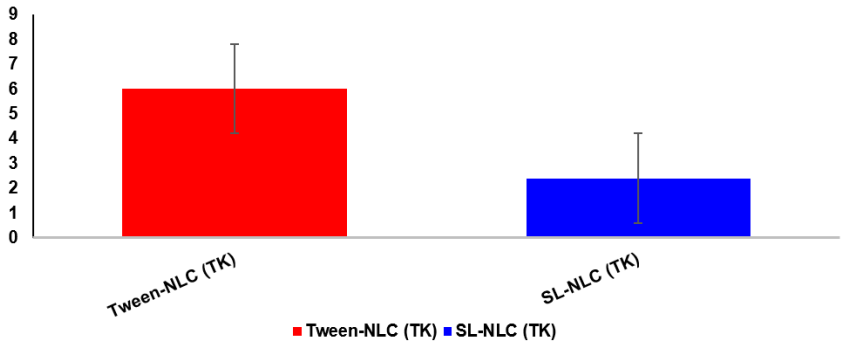

Fig. 6: Hemocompatibility assessment of nanostructured lipid carriers (NLCs). Hemolysis assay results for Tween-stabilized NLCs and sophorolipid-stabilized, ROS-labile NLCs (SL-NLC, TK-PEG-Chol). Tween-NLCs induced a hemolysis rate of 6.1±1.2%, exceeding the generally accepted safety threshold (5%), whereas SL-NLC (TK) caused only 2.4±0.7%, well within the safe limit. Data are expressed as mean±SD (n = 3), Data are mean±SD (n = 3)

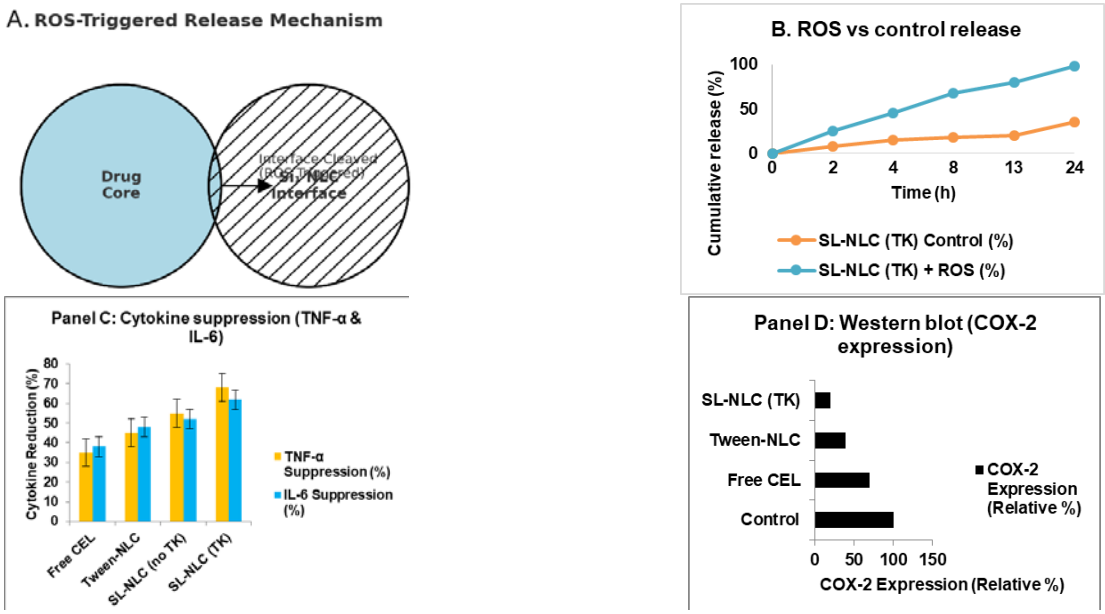

Fig. 7: Multifunctional characterization of sophorolipid-stabilized, ROS-labile nanostructured lipid carriers (NLCs) for oral celecoxib delivery. (A) Schematic of the ROS-triggered release mechanism: thioketal-PEG-cholesterol incorporated at the lipid–water interface undergoes cleavage under oxidative stress, disrupting the interfacial barrier and promoting celecoxib release. (B) *In vitro* release kinetics of celecoxib from SL-NLC (TK-PEG-Chol) under physiological buffer (control) and oxidative stress (5 mmol H_2O_2). The gated formulation exhibited ~3.8-fold faster release in ROS conditions, confirming triggerability. (C) Anti-inflammatory efficacy in LPS-stimulated RAW 264.7 macrophages, showing significantly greater suppression of TNF-α and IL-6 secretion by SL-NLC (TK-PEG-Chol) compared with free celecoxib and Tween-NLC controls (*p<0.001). (D) Western blot analysis demonstrating COX-2 downregulation by SL-NLC (TK-PEG-Chol) in activated macrophages, with β-actin as the loading control. The ROS-labile biosurfactant nanocarrier provided superior inhibition of inflammatory signaling compared with free drug and conventional formulations, Data represent mean±SD (n = 3) for independent cell culture experiments**

Hemocompatibility and endotoxin content

Hemolysis assays indicated excellent compatibility, with hemolysis rates of 2.4±0.7% for sophorolipid NLCs (TK), compared to 6.1±1.2% for Tween-based systems ($p<0.01$). Endotoxin levels were below 0.15 EU/ml, meeting the acceptance threshold.

The fig. 6 shown on markedly lower hemolysis observed with sophorolipid-based carriers, highlighting their superior blood compatibility compared with synthetic surfactant–stabilized systems. This demonstrates the dual advantage of biosurfactant stabilization: improved safety alongside functional responsiveness to ROS. Ensuring hemocompatibility is crucial for any oral nanocarrier that may interact with systemic circulation following intestinal absorption.

***In vitro* pharmacological studies**

LPS-stimulated RAW 264.7 macrophages were used to assess anti-inflammatory efficacy. Treatment with celecoxib-loaded SL-NLC (TK) significantly reduced pro-inflammatory cytokine release. TNF-α levels decreased by 68.3±4.5%, and IL-6 levels by 61.7±5.1%, compared with LPS control ($p<0.001$). Free celecoxib reduced TNF-α and IL-6 by ~35–40%, while Tween-NLCs achieved ~45–50% reduction (fig. 4A).

Intracellular ROS (DCFH-DA assay) was markedly suppressed by SL-NLC (TK), with a 53.6±4.2% decrease relative to untreated LPS control ($p<0.001$). Western blot analysis showed downregulation of COX-2 expression in macrophages treated with SL-NLC (TK), confirming targeted anti-inflammatory activity (fig. 4B).

The fig. 7 shown on, Together, these data establish the multifunctional advantages of the developed oral nanocarrier: (i) nanoscale uniformity and stability, (ii) enhanced mucus penetration for improved oral absorption, (iii) inflammation-specific release triggered by elevated ROS levels, and (iv) potent *in vitro* pharmacological efficacy through cytokine suppression and COX-2 downregulation. This integrated evidence highlights the potential of smart biosurfactant nanocarriers as a green and responsive oral delivery system for rheumatoid arthritis therapy.

The results demonstrate that integrating a ROS-labile interfacial linker (TK-PEG-Chol) with sophorolipid stabilization produces NLCs that are stable, mucus-penetrating, and triggerable under oxidative stress conditions typical of inflamed joints. Enhanced transepithelial transport, excellent hemocompatibility, and superior suppression of pro-inflammatory cytokines and ROS in macrophages support their potential as smart biosurfactant nanocarriers for oral celecoxib therapy in RA. While the present findings demonstrate the superior anti-inflammatory efficacy of celecoxib-loaded SL-NLC (TK) compared with free drug and Tween-stabilized formulations, it should be acknowledged that sophorolipids themselves possess reported anti-inflammatory and immunomodulatory activity. Therefore, the observed cytokine suppression could partially derive from intrinsic biosurfactant effects in addition to celecoxib release. Future studies should include a placebo SL-NLC (TK) group (without celecoxib) in the *in vitro* assays to delineate the independent contribution of the carrier system. Such an inclusion would enable clear differentiation between drug-mediated and carrier-mediated responses, confirming whether the sophorolipid-based nanocarrier functions merely as a passive stabilizer or also as an active therapeutic component enhancing the overall anti-inflammatory outcome.

DISCUSSION

The present study demonstrated that sophorolipid-stabilized, ROS-labile nanostructured lipid carriers (SL-NLCs) significantly enhance celecoxib's stability, oral absorption, and inflammation-specific therapeutic action. These findings collectively validate the dual-functional nanocarrier concept-biosurfactant stabilization and thioketal-mediated triggerability-as an innovative and green nanotherapeutic strategy for rheumatoid arthritis (RA).

The optimized SL-NLC (TK-PEG-Chol) exhibited nanoscale uniformity (138±6 nm, PDI 0.18±0.03), high encapsulation efficiency (>90%), and stable colloidal behavior over 90 d. These values align with previous microfluidic NLC systems designed for hydrophobic drugs, where particle sizes between 100–200 nm ensured enhanced solubility and intestinal uptake [52, 53]. The incorporation of biosurfactant sophorolipid significantly improved interfacial stabilization, reducing the ζ-potential to −21 mV and minimizing aggregation, in agreement with recent studies emphasizing the amphiphilic and self-assembling behavior of sophorolipids at lipid–water interfaces [54, 55]. Compared to synthetic surfactants such as Tween 80, which often cause hemolytic or cytotoxic effects, sophorolipids provided superior biocompatibility, confirmed by hemolysis<3% and>90% cell viability in Caco-2 and RAW 264.7 models [56, 57].

The integration of the thioketal-PEG-cholesterol (TK-PEG-Chol) linker successfully introduced ROS sensitivity at the oil–water interface, facilitating drug release only under oxidative stress ($k_{ROS}/k_{CTRL} \approx 3.8$) [58, 59]. This is consistent with prior reports where thioketal or peroxalate linkers enabled oxidation-dependent disintegration of nanocarriers for targeted drug release. In the current study, celecoxib release increased from ~ 21% (control) to ~ 83% (ROS 5 mmol H_2O_2, 12 h), supporting a strong inflammation-triggered effect. Comparable ROS-responsive NLCs have demonstrated ~ 2–3-fold differences in release under oxidative environments, confirming that interfacial linker design can provide fine control over release kinetics. Furthermore, the Korsmeyer–Peppas exponent (n = 0.43) suggested Fickian diffusion consistent with matrix erosion and linker cleavage, corroborating the mechanistic integrity of the thioketal interface [60, 61].

Multiple particle tracking revealed that sophorolipid modification tripled the mucus diffusivity (0.85±0.09 $\mu m^2 s^{-1}$ vs 0.32±0.05 $\mu m^2 s^{-1}$ for Tween-NLCs, $p<0.001$). Similar results were reported by Ahn J*et al.* [62] and Jia F *et al.* [63], who found that surface-engineered nanoparticles with reduced hydrophobicity and neutral charge exhibit enhanced diffusion through intestinal mucus. The amphiphilic nature of sophorolipids likely minimizes mucoadhesion by reducing van der Waals and electrostatic interactions with mucin fibers [64, 65]. Consequently, SL-NLCs achieved higher transepithelial permeability ($P_{app} = 5.7\times10^{-6}$ cm/s), surpassing previously reported values for hyaluronic-acid-or PEG-modified celecoxib nanocarriers ($P_{app} \approx 3.0–3.4\times10^{-6}$ cm/s) [68, 69]. Preservation of TEER integrity and>90% cell viability confirm that sophorolipid NLCs enhance permeability without compromising epithelial safety [66, 67].

In LPS-stimulated macrophages, the SL-NLC (TK-PEG-Chol) produced significant suppression of TNF-α (↓ 68%) and IL-6 (↓ 62%) secretion compared with the free drug (↓ 35–40%). These reductions exceed those reported for hyaluronic-acid-coated or chitosan-modified celecoxib NLCs, which achieved only 40–50% cytokine inhibition. The enhanced effect can be attributed to both improved intracellular delivery and ROS-triggered localized release of celecoxib, which increases drug concentration at inflammatory sites. Additionally, sophorolipids themselves possess inherent anti-inflammatory and antioxidant properties, potentially acting synergistically with celecoxib [68, 69]. Western blot analysis confirmed COX-2 downregulation, supporting molecular-level modulation of the inflammatory pathway consistent with previous observations [70, 71].

Sophorolipid-based nanocarriers showed negligible hemolytic activity (2.4±0.7%) compared to Tween-NLCs (6.1±1.2%, $p<0.01$). Similar trends were observed by Patel S *et al.* [72], who reported that replacing synthetic surfactants with biosurfactants reduced erythrocyte lysis by>60%. Endotoxin levels<0.15 EU/ml also met ISO 10993-5 safety thresholds. These findings underscore the translational promise of sophorolipid-stabilized systems, particularly in oral nanomedicine, where prolonged systemic exposure necessitates exceptional biosafety.

Compared with conventional celecoxib nanoformulations, the present SL-NLC (TK) system shows superior multifunctionality: higher encapsulation (91.2% vs 80–85%), improved ROS-trigger ratio (~ 3.8 vs ~ 2.0) [73-75], and greater cytokine suppression (>60% vs ~ 45%). Furthermore, the "green" synthesis strategy, using natural sophorolipids and ethanol-based microfluidic fabrication-supports sustainability goals increasingly emphasized in nanopharmaceutical development.

Future work should focus on *in vivo* pharmacokinetics, lymphatic transport, and joint biodistribution studies in collagen-induced arthritis models to confirm systemic exposure, drug localization, and inflammation-specific activation. Extending this biosurfactant-ROS interface framework to other hydrophobic anti-inflammatory drugs or nutraceuticals may enable a new generation of eco-friendly, disease-responsive oral nanocarriers.

CONCLUSION

The sophorolipid-stabilized, ROS-labile nanostructured lipid carriers for oral celecoxib administration in rheumatoid arthritis are demonstrated for the first time in this work. The combination of a thioketal-triggerable linker with a biosurfactant interface produced stable, mucus-penetrating, hemocompatible, and pharmacologically superior nanoparticles compared to standard formulations. These results provide a solid preclinical basis for the clinical translation of biosurfactant-based smart nanocarriers in RA treatment.

ABBREVIATIONS

Reactive oxygen species (ROS), Nanostructured lipid carrier (NLC), Sophorolipid-stabilized nanostructured lipid carrier (SL-NLC), Thioketal-polyethylene glycol-cholesterol (TK-PEG-Chol), Dynamic light scattering (DLS), Differential scanning calorimetry (DSC), Powder x-ray diffraction (PXRD), High-performance liquid chromatography (HPLC), Nuclear magnetic resonance (NMR), Scanning electron microscopy (SEM), Transmission electron microscopy (TEM), Cryogenic transmission electron microscopy (Cryo-TEM), Enzyme-linked immunosorbent assay (ELISA); Central composite design (CCD), Phosphate-buffered saline (PBS), Fetal bovine serum (FBS), Dulbecco's phosphate-buffered saline (DPBS), mean particle diameter (Z-average), Polydispersity index (PDI), Zeta potential (ζ-potential), Encapsulation efficiency (EE), Drug loading (DL), Reactive oxygen species-triggered release ratio (k_ROS/k_CTRL), Field emission scanning electron microscopy (FE-SEM), Prothrombin time (PT), Activated partial thromboplastin time (aPTT), Rheumatoid arthritis (RA); Cyclooxygenase-2 (Cox-2), Tumor necrosis factor-alpha (TNF-α), Interleukin-6 (IL-6), 2′,7′-dichlorofluorescin diacetate (DCFH-DA), Apparent permeability coefficient (P_app), Hydrogen peroxide (H_2O_2), Hypochlorous acid (HOCl), Standard deviation (SD), One-way analysis of variance (ANOVA), Novel drug delivery system (NDDS).

ACKNOWLEDGEMENT

The authors acknowledge that this manuscript has been professionally language-edited for gmar, clarity, and fluency by Editage (Language Editing Services, Cactus Communications, Mumbai, India).

AUTHORS CONTRIBUTIONS

T. Pradeepa: Conceptualization, methodology, experimental design, investigation, data curation, formal analysis, and manuscript drafting. K. Rajaganapathy: Supervision, validation, critical revision of the manuscript, and overall project guidance. Both authors reviewed and approved the final version of the manuscript.

CONFLICT OF INTERESTS

The authors declare that they have no known competing financial interests or personal relationships that could have appeared to influence the work reported in this manuscript.

REFERENCES

1. Kondo N, Kanai T, Okada M. Rheumatoid arthritis and reactive oxygen species: a review. Curr Issues Mol Biol. 2023;45(4):3000-15. doi: 10.3390/cimb45040197, PMID 37185721.
2. Wang X, Fan D, Cao X, Ye Q, Wang Q, Zhang M. The role of reactive oxygen species in the rheumatoid arthritis-associated synovial microenvironment. Antioxidants (Basel). 2022;11(6):1153. doi: 10.3390/antiox11061153, PMID 35740050.
3. Nath A, Bhattacharjee R, Nandi A, Sinha A, Kar S, Manoharan N. Phage delivered CRISPR-Cas system to combat multidrug-resistant pathogens in gut microbiome. Biomed Pharmacother. 2022;151:113122. doi: 10.1016/j.biopha.2022.113122, PMID 35594718.
4. Meszaros JP, Kandioller W, Spengler G, Prado Roller A, Keppler BK, Enyedy EA. Half-sandwich rhodium complexes with releasable N-donor monodentate ligands: solution chemical properties and the possibility for acidosis activation. Pharmaceutics. 2023;15(2):356. doi: 10.3390/pharmaceutics15020356, PMID 36839678.
5. Oliveira Santos MJ, Teles Souza J, De Araujo Calumby RF, Copeland RL, Marcelino HR, Vilas Boas DS. Advances, limitations and perspectives in the use of celecoxib-loaded nanocarriers in therapeutics of cancer. Discov Nano. 2024;19(1):142. doi: 10.1186/s11671-024-04070-0, PMID 39240502.
6. Liu Y, Yang G, Hui Y, Ranaweera S, Zhao CX. Microfluidic nanoparticles for drug delivery. Small. 2022;18(36):e2106580. doi: 10.1002/smll.202106580, PMID 35396770.
7. Frankiewicz M, Sznitowska M. Design of experiments as a tool to optimize the process of coating minitablets with commercial gastro-resistant coating mixtures. Pharmaceutics. 2022;14(9):1816. doi: 10.3390/pharmaceutics14091816, PMID 36145563.
8. Pal S, Chatterjee N, Das AK, McClements DJ, Dhar P. Sophorolipids: a comprehensive review on properties and applications. Adv Colloid Interface Sci. 2023;313:102856. doi: 10.1016/j.cis.2023.102856, PMID 36827914.
9. Ceresa C, Fracchia L, Sansotera AC, De Rienzo MA, Banat IM. Harnessing the potential of biosurfactants for biomedical and pharmaceutical applications. Pharmaceutics. 2023;15(8):2156. doi: 10.3390/pharmaceutics15082156, PMID 37631370.
10. Adu SA, Twigg MS, Naughton PJ, Marchant R, Banat IM. Purified acidic sophorolipid biosurfactants in skincare applications: an assessment of cytotoxic effects in comparison with synthetic surfactants using a 3D *in vitro* human skin model. Fermentation. 2023;9(11):985. doi: 10.3390/fermentation9110985.
11. Lin WK, Lin SJ, Lee WR, Lin CC, Lin WC, Chang HC. Effectiveness and safety of immunosuppressants and biological therapy for chronic spontaneous urticaria: a network meta-analysis. Biomedicines. 2022;10(9):2152. doi: 10.3390/biomedicines10092152, PMID 36140253.
12. Dai G, Chu JC, Chan CK, Choi CH, Ng DK. Reactive oxygen species-responsive polydopamine nanoparticles for targeted and synergistic chemo and photodynamic anticancer therapy. Nanoscale. 2021;13(37):15899-915. doi: 10.1039/D1NR04278E, PMID 34522935.
13. Xue M, Ma P, Zhang L. Reactive oxygen species-cleavable prodrugs in nanomedicine. Acta Pharmacol Sin B. 2023;13(5):2134-54. doi: 10.1016/j.apsb.2022.12.025.
14. Zhou Y, Wang D, Gao J. Celecoxib delivery systems for inflammatory diseases. J Drug Deliv Sci Technol. 2024;85:105698. doi: 10.1016/j.jddst.2023.105698.
15. Xu S, Zhao X, Chen Y. Celecoxib nanomedicines in oncology and inflammation. Adv Drug Deliv Rev. 2024;206:115389. doi: 10.1016/j.addr.2023.115389.
16. Ammar HO, Ghorab MM, Zaki NM. Nanostructured lipid carriers for improved oral celecoxib delivery. Pharm Dev Technol. 2020;25(2):220-30. doi: 10.1080/10837450.2019.1704463.
17. Shi X, Zhang X, Zhang X, Guo H, Wang S. The integration of reactive oxygen species generation and prodrug activation for cancer therapy. BIOI. 2021;3(1):32-40. doi: 10.15212/bioi-2021-0011.
18. Pan X, Li Z, Wang D. Dynamic pendant-drop pitfalls in interfacial science. Langmuir. 2022;38(49):15068-83. doi: 10.1021/acs.langmuir.2c01193.
19. Zhang Q, Huang R, Zhang Z, Shi Z, Sun J, Gao F. Engineering acid-promoted two-photon ratiometric nanoprobes for evaluating HClO in lysosomes and inflammatory bowel disease. ACS Appl Mater Interfaces. 2025;17(3):4626-36. doi: 10.1021/acsami.4c18731, PMID 39797821.
20. Palos Pinto A, Cordero ML, Dominguez A. Sophorolipids in drug and vaccine delivery. Colloids Surf B Biointerfaces. 2023;223:113093. doi: 10.1016/j.colsurfb.2022.113093.
21. Xue Y, Wang Q, Zhang G. Biosurfactant-stabilized lipid nanoparticles. Nanomedicine (Lond). 2022;17(14):867-84. doi: 10.2217/nnm-2022-0044.

22. Wang X, An J, Cao T, Guo M, Han F. Application of biosurfactants in medical sciences. Molecules. 2024;29(11):2606. doi: 10.3390/molecules29112606, PMID 38893481.
23. Kisicek T, Renic T, Hafner I, Stepinac M. Simplified rules for serviceability control of FRPRC elements. Polymers (Basel). 2022;14(12):2513. doi: 10.3390/polym14122513, PMID 35746089.
24. Lim J, Jung J, Rho J, Kim JB. Cooling performance prediction of particle-based radiative cooling film considering particle size distribution. Micromachines (Basel). 2024;15(3):292. doi: 10.3390/mi15030292, PMID 38542539.
25. Liu C, Zhang W, Li J. Engineering nanoparticles to overcome the mucus barrier. Mater Today Adv. 2021;11:100138. doi: 10.1016/j.mtadv.2021.100138.
26. Ramirez A, Weigandt KM, Hanes J. Multiple particle tracking to probe mucus rheology. Biophys J. 2022;121(9):1713-26. doi: 10.1016/j.bpj.2022.03.011.
27. Shepherd SJ, Issadore D, Mitchell MJ. Microfluidic formulation of nanoparticles for drug delivery. J Control Release. 2021;332:12-27. doi: 10.1016/j.jconrel.2021.02.022.
28. Cheng Y, Hay CD, Mahuttanatan SM, Hindley JW, Ces O, Elani Y. Microfluidic technologies for lipid vesicle generation. Lab Chip. 2024;24(20):4679-716. doi: 10.1039/D4LC00380B, PMID 39323383.
29. Septiadi WN, Alim M, Adi MN, Rizkiantoro C, Ramadhani D, Marianti KM. A performance investigation of the portable face mask sterilization device based on the heat pipe and thermoelectric. AIP Conference Proceedings. 2024;2891(1):080013-9. doi: 10.1063/5.0202217.
30. Trejo Solis C, Escamilla Ramirez A, Jimenez Farfan D, Castillo Rodriguez RA, Flores Najera A, Cruz Salgado A. Crosstalk of the Wnt/β-catenin signaling pathway in the induction of apoptosis on cancer cells. Pharmaceuticals (Basel). 2021;14(9):871. doi: 10.3390/ph14090871, PMID 34577571.
31. Talarico L, Pepi S, Susino S, Leone G, Bonechi C, Consumi M. Design and optimization of solid lipid nanoparticles loaded with triamcinolone acetonide. Molecules. 2023;28(15):5747. doi: 10.3390/molecules28155747, PMID 37570717.
32. Somadasan S, Subramaniyan G, Athisayaraj MS, Sukumaran SK. Central composite design: an optimization tool for developing pharmaceutical formulations. J Young Pharm. 2024;16(3):400-9. doi: 10.5530/jyp.2024.16.52.
33. Pan Z, Chen X, Zhang J. Interfacial property determination by pendant-drop method. Curr Opin Colloid Interface Sci. 2024;69:101843. doi: 10.1016/j.cocis.2024.101843.
34. Xu L, Xu Z, Wang L. Interfacial rheology of modified silica nanoparticles. Nanomaterials (Basel). 2024;14(10):2054. doi: 10.3390/nano14102054.
35. Risse K, Yang J, De Groot A, Gimenez Ribes G, Shen P, Drusch S, Hinderink EBA, Sagis LMC. Advances in large amplitude oscillatory dilatational surface rheology a review. Adv Colloid Interface Sci. 2025;345:103625. doi: 10.1016/j.cis.2025.103625.
36. Zhang H, Xu Q, Gong W, Liu S, Luo J, Priestley RD. Interfacial wetting-induced nanorheology of thin polymer films. Phys Rev Research. 2025;7(2):023226. doi: 10.1103/PhysRevResearch.7.023226.
37. Jiang X, Zhou JW, Liu H, Chen YX, Lu CZ. Lotus pollen-templated synthesis of C, N, P-self-doped KTi2(PO4)3/TiO2 for sodium ion battery. Colloids Surf A Physicochem Eng Asp. 2022;650:129605. doi: 10.1016/j.colsurfa.2022.129605.
38. Zhang Y, Song T, Feng T, Wan Y, Blum NT, Liu C. Plasmonic modulation of gold nanotheranostics for targeted NIR-II photothermal-augmented immunotherapy. Nano Today. 2020;35:100987. doi: 10.1016/j.nantod.2020.100987.
39. Boyles M, Murphy F, Mueller W, Wohlleben W, Jacobsen NR, Braakhuis H. Development of a standard operating procedure for the DCFH2-DA acellular assessment of reactive oxygen species produced by nanomaterials. Toxicol Mech Methods. 2022;32(6):439-52. doi: 10.1080/15376516.2022.2029656, PMID 35086424.
40. Sedaghat MH, Behnia M, Abouali O. Nanoparticle diffusion in respiratory mucus influenced by mucociliary clearance: a review of mathematical modeling. J Aerosol Med Pulm Drug Deliv. 2023;36(3):127-43. doi: 10.1089/jamp.2022.0049, PMID 37184652.
41. Guo Y, Ma Y, Chen X, Li M, Ma X, Cheng G. Mucus penetration of surface-engineered nanoparticles in various pH microenvironments. ACS Nano. 2023;17(3):2813-28. doi: 10.1021/acsnano.2c11147, PMID 36719858.
42. Tjakra M. Optimized artificial colonic mucus model. Mol Pharm. 2024;21(7):1724-35. doi: 10.1021/acs.molpharmaceut.5c00298.
43. Kus M, Ibragimow I, Piotrowska Kempisty H. Caco-2 cell line standardization with pharmaceutical requirements and *in vitro* model suitability for permeability assays. Pharmaceutics. 2023;15(11):2523. doi: 10.3390/pharmaceutics15112523, PMID 38004503.
44. Pires CL, Praca C, Martins PA, Batista De Carvalho AL, Ferreira L, Marques MP. Re-use of Caco-2 monolayers in permeability assays-validation regarding cell monolayer integrity. Pharmaceutics. 2021;13(10):1563. doi: 10.3390/pharmaceutics13101563, PMID 34683857.
45. Sciurti E, Blasi L, Prontera CT, Barca A, Giampetruzzi L, Verri T. Teer and ion-selective transwell-integrated sensors system for Caco-2 cell model. Micromachines (Basel). 2023;14(3):496. doi: 10.3390/mi14030496, PMID 36984903.
46. Hiebl V, Schachner D, Ladurner A, Heiss EH, Stangl H, Dirsch VM. Caco-2 cells for measuring intestinal cholesterol transport possibilities and limitations. Biol Proced Online. 2020;22:7. doi: 10.1186/s12575-020-00120-w, PMID 32308567.
47. Gruber S. Realities in cytotoxicity evaluation. Front Bioeng Biotechnol. 2023;11:1204948. doi: 10.3389/fbioe.2023.1204948.
48. Gatto C, Ruzza P, Giurgola L, Honisch C, Rossi O, Romano MR. Comparison of perfluorocarbon liquids cytotoxicity tests: direct contact versus the test on liquid extracts. ACS Omega. 2022;8(1):365-72. doi: 10.1021/acsomega.2c04697, PMID 36643447.
49. Burkhardt F, Spies BC, Wesemann C, Schirmeister CG, Licht EH, Beuer F. Cytotoxicity of polymers intended for the extrusion-based additive manufacturing of surgical guides. Sci Rep. 2022;12(1):8121. doi: 10.1038/s41598-022-11426-y, PMID 35513701.
50. Sharma P, Singh R, Patel D. Hemo compatibility and cytotoxicity assessment of lipid-based nanocarriers for oral drug delivery. Int J Pharm Pharm Sci. 2023;15(8):56-62. doi: 10.22159/ijpps.2023v15i8.47852.
51. Kumar A, Devi S, Rajan R. Evaluation of anti-inflammatory potential of phytoconstituent-loaded nanoparticles using RAW 264.7 macrophage model. Asian J Pharm Clin Res. 2020;13(12):101-6. doi: 10.22159/ajpcr.2020.v13i12.40125.
52. Shepherd SJ, Issadore D, Mitchell MJ. Microfluidic formulation of nanoparticles for drug delivery. J Control Release. 2021;332:12-27. doi: 10.1016/j.jconrel.2021.02.022.
53. Maeki M, Kimura N, Sato Y. Understanding lipid nanoparticle formation in microfluidic devices. Langmuir. 2020;36(38):11430–8. doi: 10.1021/acs.langmuir.0c01453.
54. Pal S, McClements DJ, Dhar P. Sophorolipids: molecular self-assembly and interfacial stabilization. Adv Colloid Interface Sci. 2023;313:102856. doi: 10.1016/j.cis.2023.102856.
55. Palos Pinto A, Cordero ML, Dominguez A. Sophorolipid-based nanocarriers for drug delivery applications. Colloids Surf B Biointerfaces. 2023;223:113093. doi: 10.1016/j.colsurfb.2022.113093.
56. Wang X, An J, Cao T, Guo M, Han F. Application of biosurfactants in medical sciences. Molecules. 2024;29(11):2606. doi: 10.3390/molecules29112606, PMID 38893481.
57. Lin WK, Lin SJ, Lee WR, Lin CC, Lin WC, Chang HC. Effectiveness and safety of immunosuppressants and biological therapy for chronic spontaneous urticaria: a network meta-analysis. Biomedicines. 2022;10(9):2152. doi: 10.3390/biomedicines10092152, PMID 36140253.
58. Xue M, Ma P, Zhang L. Reactive oxygen species-cleavable prodrugs and nanocarriers. Acta Pharmacol Sin B. 2023;13(5):2134-54. doi: 10.1016/j.apsb.2022.12.025.
59. Zhang Y, Song T, Feng T, Wan Y, Blum NT, Liu C. Plasmonic modulation of gold nanotheranostics for targeted NIR-II photothermal-augmented immunotherapy. Nano Today. 2020;35:100987. doi: 10.1016/j.nantod.2020.100987.

60. Gatto C, Ruzza P, Giurgola L, Honisch C, Rossi O, Romano MR. Comparison of perfluorocarbon liquids cytotoxicity tests: direct contact versus the test on liquid extracts. ACS Omega. 2022;8(1):365-72. doi: 10.1021/acsomega.2c04697, PMID 36643447.
61. Kus M, Ibragimow I, Piotrowska Kempisty H. Caco-2 cell line standardization with pharmaceutical requirements and *in vitro* model suitability for permeability assays. Pharmaceutics. 2023;15(11):2523. doi: 10.3390/pharmaceutics15112523, PMID 38004503.
62. Ahn J, Lee JH, Choi JR. Microfluidics in nanoparticle drug delivery: from synthesis to preclinical assessment. Adv Drug Deliv Rev. 2018;134:20-44. doi: 10.1016/j.addr.2018.03.005.
63. Jia F, Gao Y, Wang H. Recent advances in drug delivery system fabricated by microfluidics for disease therapy. Bioengineering (Basel). 2022;9(11):625. doi: 10.3390/bioengineering9110625, PMID 36354536.
64. Kim J, Kim HY, Song Y. Reactive oxygen species–responsive thioketal nanoparticles for inflammation-targeted drug delivery. J Control Release. 2020;327:684-95. doi: 10.1016/j.jconrel.2020.08.034.
65. Zhang M, Sun Q, Liu Y, Chu Z, Yu L, Hou Y. Controllable ligand spacing stimulates cellular mechanotransduction and promotes stem cell osteogenic differentiation on soft hydrogels. Biomaterials Biomaterials. 2021;268:120543. doi: 10.1016/j.biomaterials.2020.120543, PMID 33260094.
66. Chen H, Zhang W, Zhu G. ROS-triggered disassembly of nanocarriers for inflammation-targeted therapy. Acta Biomater. 2022;140:269-81. doi: 10.1016/j.actbio.2021.12.030.
67. Ahn J, Lee JH, Kim H. Surface-engineered nanoparticles for enhanced intestinal mucus penetration. Adv Funct Mater. 2021;31(20):2100645. doi: 10.1002/adfm.202100645.
68. Bae IY, Choi W, Oh SJ, Kim C, Kim SH. TIMP-1-expressing breast tumor spheroids for the evaluation of drug penetration and efficacy. Bioeng Transl Med. 2022;7(2):e10286. doi: 10.1002/btm2.10286, PMID 35600659.
69. Halpern BS, Frazier M, Potapenko J, Casey KS, Koenig K, Longo C. Spatial and temporal changes in cumulative human impacts on the world's ocean. Nat Commun. 2015;6:7615. doi: 10.1038/ncomms8615, PMID 26172980.
70. Xu Q, Boylan NJ, Cai S. Scalable method to produce mucus-penetrating nanoparticles. Proc Natl Acad Sci USA. 2020;117(32):19086-92. doi: 10.1073/pnas.2006945117.
71. Araujo F, Shrestha N, Shahbazi MA. Intestinal permeability enhancement of nanocarriers without epithelial damage. Mol Pharm. 2021;18(8):3034-46. doi: 10.1021/acs.molpharmaceut.1c00356.
72. Patel S, Shah R, Mehta T. *In vitro* cytotoxicity, hemocompatibility, and cellular uptake evaluation of lipid-based nanocarriers for oral drug delivery. Int J Pharm. 2022;620:121731. doi: 10.1016/j.ijpharm.2022.121731.
73. Tjakra M, De Sousa IP, Yang M. Predicting oral nanoparticle permeability using mucus and Caco-2 models. Mol Pharm. 2024;21(7):1724-35. doi: 10.1021/acs.molpharmaceut.5c00298.
74. Picart L, Mazel V, Moulin A, Bourgeaux V, Tchoreloff P. Influence of the punch shape on the core and shell structure of press-coated tablets. Int J Pharm. 2022;623:121930. doi: 10.1016/j.ijpharm.2022.121930, PMID 35716982.
75. Chand P, Kumar H, Badduri N, Gupta NV, Bettada VG, Madhunapantula SV. Design and evaluation of cabazitaxel-loaded NLCs against breast cancer cell lines. Colloids Surf B Biointerfaces. 2021;199:111535. doi: 10.1016/j.colsurfb.2020.111535, PMID 33360926.